The Effect of Boron Doping Concentration on the Electrochemical Oxidation of Chlorine Using BDD Electrode

Journal of The Electrochemical Society

The Effect of Boron Doping Concentration on the Electrochemical Oxidation of Chlorine Using BDD Electrode

To cite this article before publication: Zhishen Li *et al* 2022 *J. Electrochem. Soc.* in press https://doi.org/10.1149/1945-7111/acad2d

The Effect of Boron Doping Concentration on the Electrochemical Oxidation of Chlorine Using BDD Electrode

Journal:	*Journal of The Electrochemical Society*
Manuscript ID	JES-108449.R1
Manuscript Type:	Research Paper
Date Submitted by the Author:	15-Nov-2022
Complete List of Authors:	Li, Zhishen; Central South University Zhou, Bo; Queen Mary University of London Yang, Wanlin; Central South University Deng, Zejun; Central South University Chen, Fenglei; Central South University Bai, Hena; Central South University P. E, Sharel ; University of Edinburgh School of Engineering Ma, Li; Central South University Wei, Qiuping; Central South University,
Keywords:	Boron-doped diamond, Electrochemical Advanced Oxidation Processes, oxychlorine by-products

The Effect of Boron Doping Concentration on the Electrochemical Oxidation of Chlorine Using BDD Electrode

Li zhishen,[1] Zhou bo,[2,z] Yang wanlin,[1] Deng zejun,[1] Chen fenglei,[1] Bai hena,[3] Sharel P. E,[3] Ma li,[4] and Wei quipping[1,z]

[1]School of Materials Science and Engineering, Central South University, Changsha 410083, People's Republic of China
[2]School of Engineering and Materials Science, Queen Mary University of London, London E1 4NS, UK
[3]School of Engineering | University of Edinburgh, Edinburgh, EH9 3DW, UK
[4]State Key Laboratory of Powder Metallurgy, Central South University, Changsha 410083, People's Republic of China

[z]E-mail: b.zhou@qmul.ac.uk; qiupwei@csu.edu.cn

Abstract

Boron-doped diamond (BDD) electrode is an excellent candidate for anodic electrochemical oxidation of wastewater. However, higher concentrations of ClO_3^- and ClO_4^- of biotoxicity was found during chloride electrolysis using BDD electrodes compared to other electrode materials. In this study, BDD electrodes with five different boron doping concentrations were fabricated on silicon substrates using hot-filament chemical vapor deposition (HFCVD) method. The physical and electrochemical characterisation were conducted, which confirmed that with the decrease of boron concentration, the crystal size of the diamond decreased, oxygen evolution potential decreased, charge transfer resistance decreased while the electro-active surface area (EASA) increased. The electrochemical oxidation experiments of NaCl solution were carried out with these five BDD electrodes and time-dependent traces of product concentrations, current efficiencies and energy consumptions were compared and discussed. When the boron concentration increased, the minimum energy required to produce unit active chlorine (AC) decreased initially then increased, the same tendency was found in the yields of ClO_3^- and ClO_4^-. The lightly doped BDD (1.23×10^{20} cm^{-3}) showed low energy consumption and high yield of AC, and low yields of ClO_3^- and ClO_4^-. Electrolysis of chlorine-containing organic wastewater was studied which further demonstrated the good performance of lightly doped BDD electrode.

1.Introduction

Electrochemical Advanced Oxidation Processes (EAOPs) have been established as powerful tools in wastewater treatment by oxidizing pollutants directly on the anode surface or oxidizing them indirectly via electrogenerated highly oxidizing species (*e.g.* active chlorine[1, 2], hydroxyl radical)[3-6]. It was found that the surface properties of the anode materials are deciding factors in the mineralization efficiency and energy consumption[7]. Compared to the conventional dimensional stable anode (DSA)[6, 8, 9], titanium and graphite electrodes[10, 11], Boron-doped diamond (BDD) electrodes exhibit extraordinary electrochemical properties including high oxygen evolution potentials, low background currents and the ability to maintain high current efficiency under high voltage, which enable rapid removals of most organic pollutants with low energy consumptions[12-14]. The excellent stability of BDD has been demonstrated by its low adsorption properties, and excellent resistance in extreme acidic and basic environments[15, 16], proving that it is applicable to a wide range of water treatment environments as an ideal anode material for EAOPs.

However, the possibility to form ClO_3^- and ClO_4^- with concentrations exceed the safety range must be carefully considered when applying BDD in organic wastewater containing chlorine species[17, 18]. ClO_3^- is one of the causes of neurological, cardiovascular and respiratory toxicity and thyroid damage-induced anemia, and its toxicity could result in the loss of sperm count and mobility[19]. The results of animal experiments showed that ClO_4^- could cause histopathological changes in the thyroid gland and changes in hormone levels, and affect other system functions such as nerves, reproduction, and immunity[20]. Since Cl^- widely exists in organic sewage, domestic water, medical water, rainwater and other water bodies, the generation of toxic substances in the water treatment processes has severely limited the application prospects of BDD electrodes[21].

Many researchers have investigated the mechanisms of the formation of ClO_3^- and ClO_4^- during the BDD electrolysis. Hubler et al.[22] found that the chemically absorbed $ClO\cdot$ or $ClO_2\cdot$ could react with $OH\cdot$ to generate ClO^- or ClO_2^- and subsequently form $\equiv C\text{-}O\cdot$ and $= C\cdot OH$ sites on the BDD surface. These sites react with $ClO\cdot$ or $ClO_2\cdot$ to form chemisorbed intermediates which can then be converted to higher oxidation states

ClO_2^- and ClO_3^- by reacting with OH·. Azizi et al.[23] studied the mechanism of the formation of ClO_3^- and ClO_4^- on BDD using a rotating disk electrode combined with density functional theory (DFT) simulation. It was found that ClO_3^- was first adsorbed on the surface of the BDD film, oxidized to ClO_3· through direct electron transfer, and then oxidized to ClO_4^- by reacting with hydroxyl radicals. Long et al. [22] conducted photocatalysis of Cl^- containing solution to generate excess ·OH but no ClO_4^- was detected , which verified the two-step generation of ClO_4^- on the BDD electrode, as shown in equations (1) and (2). Afterwards, the electrochemical oxidation of NaCl solution was carried out using the BDD electrode, and it was found that the yield of free ·OH was the key factor for the second-step reaction.

$$ClO_3^- (BDD) \rightarrow ClO_3 \cdot + e^- \quad (1)$$

$$ClO_3 \cdot + \cdot OH \rightarrow ClO_4^- + H^+ \quad (2)$$

The question of how to restrain the formation of ClO_3^- and ClO_4^- during BDD electrolysis has become the focus of research in recent years. Jung et al. found that pH value can affect the synthesis of Cl_2 to inhibit the further oxidation of ClO^- thus hindering the formation of toxic substances[24]. Bergmann of Anhalt university has found that when using electrocatalytic synthesized chlorine-containing disinfectants to disinfect tap water, the higher the flow rate, the initial Cl^- concentration and the lower the current density, the lower the concentration of toxic substances (ClO_3^- and ClO_4^-) generated[25]. Nevertheless, in practice, these regulations mean a huge increase in cost, which is not favourable for industrial applications. Therefore, regulating the intrinsic properties of BDD electrode by studying the effects of substrate materials[26], sp^3/sp^2 ratio, surface terminates[27, 28] and boron doping concentration on the yield of ClO_3^- and ClO_4^- is more crucial.

The physicochemical properties of the BDD electrode have a severe impact on the products of electrochemical oxidation, and the graphite phase has a greater impact due to its high reactivity. Souzd et al.[29] performed electrochemical oxidation of 2,4-D using BDD electrodes with different sp^3/sp^2 ratios. They detected a large amount of ClO_4^- in the treated solution and found that its yield and maximum concentration were strongly related to sp^3/sp^2 ratio. Nascimento Brito et al.[30] compared the electrochemical properties of BDD electrodes with two sp^3/sp^2 ratios and carried out the electrochemical oxidation of NaCl solution. The results showed that dissolved Cl_2, ClO_2^-, ClO_2, ClO_3^- and ClO_4^- can be formed on both BDD electrodes. However, the concentration of

products changed in different manners indicating that sp^3/sp^2 ratio plays a key role in the electrochemical reaction of ClO_3^- and ClO_4^-.

Boron doping concentration also affects the physicochemical properties of BDD films. On one hand, boron doping concentration greatly affects the concentration of defects which determines the electrical properties of BDD film. On the other hand, boron doping concentration influences the deposition and growth of the BDD film, thereby changing the grain size, sp^3/sp^2 ratio etc. Santos et al. [31] explored the production of oxidizing species in chlorine-containing solutions by using commercial BDD anodes with different doing levels (100-8000 ppm). Results showed that a low doping level favours the formation of OH· while heavy doping facilitates the direct electrochemical oxidation of Cl^-. The low boron doping is also beneficial to the formation of chloride and sulphate oxidizing species during prolonged electrolysis at high current densities. These results could be attributed to the fact that BDD electrodes promoted the generation of OH·, which can effectively enhance the production of these oxidizing species. However, this study only compared the ClO_4^- yields with two boron doping concentrations and did not systematically analyse the formation of ClO_3^- and ClO_4^-.

In this work, the effects of boron doping concentration on the physical and electrochemical properties of BDD electrode were investigated with five different BDD electrodes. By testing these BDD electrodes in electrochemical oxidation of NaCl solution, the influence of boron doping concentration on the production of active chlorine (Cl_2, ClO_2^-, ClO_2), ClO_3^- and ClO_4^- was systematically explored, current efficiencies, energy consumptions and average tank voltages were also revealed by time-dependent traces. In addition, the electrochemical oxidation of chlorine-containing organic wastewater was investigated using two representative BDD electrodes with different B doping levels. These results will facilitate the easy control of chlorinated products and elucidate a safe and efficient way of using BDD electrode for chlorine-containing organic wastewater.

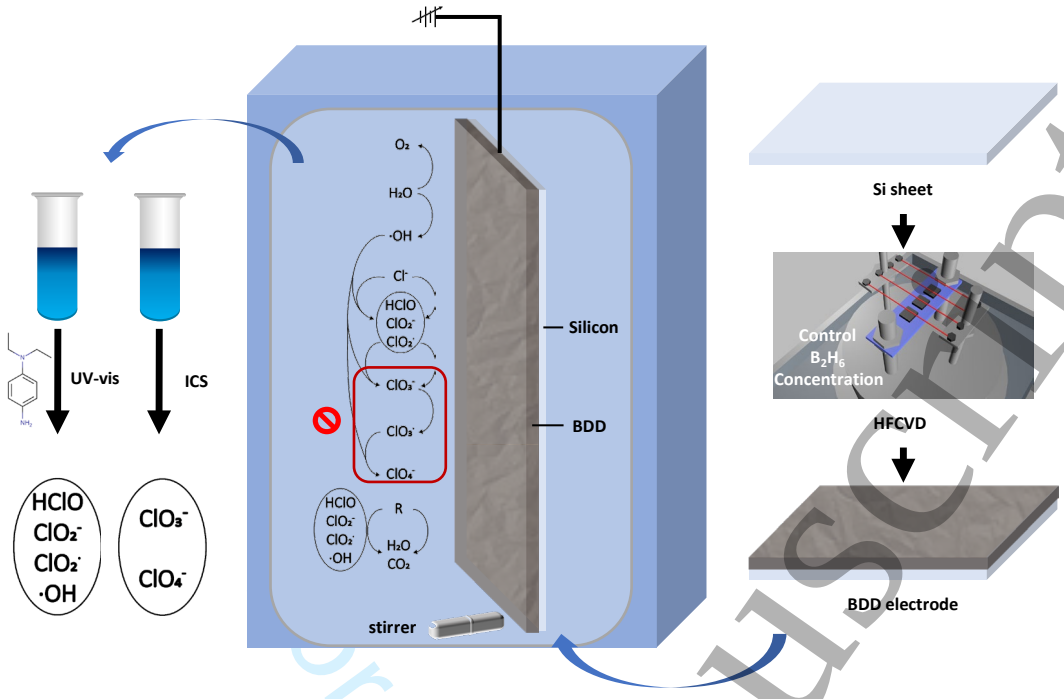

Figure 1. Schematic of experiment process and the quantification method of the AC, ClO_3^- and ClO_4^- concentrations in aqueous solution (left panel), and the preparation process of BDD electrode with different boron concentrations.

2. Experimental

2.1 The preparation of BDD electrodes

BDD electrodes were prepared using a custom-made HFCVD instrument which consists of four parallel spiral filaments (side length of 10 mm). P-type doped monocrystalline silicon (20 × 25 × 1 mm) was cleaned with acetone and absolute ethanol (analytical grade) followed by ultrasonication treatment in a diamond suspension (particle size 5-10 nm, pH 5-8) for 15 min, then the Si wafers were placed in an HFCVD chamber. For chemical vapor deposition, four heating wires with a spacing of 10 mm were used, and the distance between the heating wires and the substrate is 8 mm. A mixture of CH_4, B_2H_6 (diluted to 5% v/v with hydrogen) and H_2 was used as a gas source with a ratio H_2: B_2H_6: CH_4 = 97: x: 3.0 (sccm), and the pressure was maintained at 3 kPa. X varies in 0, 0.2, 0.6, 1.0, 1.4, 1.8, 4.0. The difference between the detection and characterization results of some similar B_2H_6 concentrations is not obvious. In order to clearly show the influence of B doping concentration, the analysis is carried out by ultra-light (0-0.1 sccm), light (0.1-0.4 sccm), medium (0.4-1.2 sccm), heavy (1.2-2.0 sccm), and ultra-heavy (4.0 sccm) B doping concentrations.

2.2 BDD characterisation

The BDD morphologies were characterized by Nova Nano SEM 230 field emission Scanning Electron Microscope (FEI, Netherlands). The boron doping concentration and sp^3/sp^2 ratio of BDD films were detected by LabRAM HR800 laser micro Raman spectrometer (Jobin Yvon, France) with the excitation wavelength of 532 nm. The electrochemical performance was detected by CHI660E electrochemical workstation (Shanghai Chenhua Company, China). The CV was tested in a standard three-electrode system (a platinum electrode and an Ag/AgCl electrode were used as the counter electrode and reference electrode, respectively). The CV curves were tested in 0.05 M H_2SO_4 solution at 100 mV s^{-1} scan rate and in 1 mM $K_4[Fe(CN)_6]/K_3[Fe(CN)_6]$ + 1 M KCl solution at a scan rate of 2, 5, 10, 15, 2, 5, 10, 15 and 20 mV s^{-1}. The EIS of the BDD electrode was measured in 1 mM $K_4[Fe(CN)_6]/K_3[Fe(CN)_6]$ + 1 M KCl solution. To eliminate the influence such as surface terminal and sp^2 phase, anodic polarization was performed in 0.1 M H_2SO_4 solution in constant voltage 5 V for 30 min before electrochemical detection and water treatment[32].

2.3 Water treatment

The electrolyte used in the electro-catalysis process was 0.1 M NaCl solution. The simulated wastewater is tetracycline (TC) and glucose (GLu) with a concentration of 0.1 g L^{-1}. BDD and stainless steel were used as the anode and cathode, respectively. The exposed surface of BDD electrodes is 20 × 25 mm^2 and the cell volume is 0.5 L. The distance between the electrodes (cathode and anode) in the degradation system is 10 mm. The speed of the magnetic stirrer (WH220-HT, WIGGENS, Germany) at the bottom of the electrolytic cell was set to 150 rpm. The current density and intensity of the DC output power supply (RD-3020, Suzhou, Wanruida) used in the electro-catalysis process are 40 mA cm^{-2} and 0.2 A.

2.4 Liquid detection

The active chlorine (AC) concentration is measured by the DPD method, where the AC concentration refers to the concentration of equivalent Cl_2 that strong oxidizing chlorine species (such as Cl_2, HClO, ClO_2^-, ClO_2) in the water sample could convert into. In this work, the ICS-3000 high performance ion chromatograph (Thermo Fisher

Scientific) was used to measure the ion concentration of ClO_3^- and ClO_4^- in water samples. Type UV-8000S ultraviolet and visible spectrophotometer (UV-vis) was used to detect electrogenerated products in water samples.

The energy consumption per unit of AC production (EC_{AC}) and the energy consumption per unit of TOC removal (EC_{TOC}) can characterize the catalytic oxidation efficiency of the BDD electrode[33]. The calculation formula is as follows:

$$EC_{\mathrm{AC}}\ (kWh\ (g_{AC})^{-1}) = \frac{UIt}{Vc_{\mathrm{t}}} \quad (3)$$

$$EC_{\mathrm{TOC}}\ (kWh\ (g_{TOC})^{-1}) = \frac{UIt}{V(TOC_0 - TOC_{\mathrm{t}})} \quad (4)$$

Where U (unit: V) is the average cell voltage during the electrochemical oxidation, I (unit: A) is the current value during the electrochemical oxidation, t (unit: h) is the electrochemical oxidation time, V (unit: A) is the volume of the solution in the electrolytic cell, c_t (unit: mg L^{-1}) is the AC concentration in the water sample when the electrochemical oxidation time is t.

Current efficiency refers to the ratio of the actual target reaction material on the electrode surface to the theoretical value of all electrons participating in the target reaction during the electrochemical process. It is an important indicator for evaluating the efficiency of the electrochemical reaction. The calculation formula is as follows[34]:

$$Current\ Efficiency\ (\%) = \frac{nFV\Delta C}{MIt \times 1000} \times 100 \quad (5)$$

where n is the number of electrons required to react per mole of species, F (unit: C mol^{-1}) is the Faraday constant, V (unit: L) is the volume of the reaction solution, and ΔC (unit: mg L^{-1}) is The amount of change in concentration when the electrochemical oxidation time is t, M (unit: g mol^{-1}) is the molar mass of the reactant, I (unit: A) is the current value during the electrochemical oxidation, t (unit: s) is the duration of the electrochemical oxidation.

3. Results and discussion

3.1 material characterisation

Figure 2a shows the SEM images of the ultra-light, light, medium, heavy, and ultra-heavy boron-doped BDD films, respectively. The films are continuous and dense indicating a good quality of the diamond. The grain size of the BDD film was measured and counted, and the results are shown in Figure 2c. It can be seen from the figure that with the increase of B/C, the median grain size decreases from 1.42 μm to 0.4 μm. This is due to the enhanced pyrolysis of B atoms with the increase of B/C, which reduces

the growth rate of diamond and increases the nucleation rate of BDD[35], causing secondary nucleation. On the other hand, B atoms can etch the diamond[36], leading to the reduction in grain size, which is especially pronounced at ultra-heavy BDD. In addition, the grain size of lightly doped and moderately doped BDD films fluctuates greatly, while the medians of grain size of these two are not much different. This shows that when B/C in the gas flow rate is 3300 - 40000 ppm, B atoms have a less inhibiting effect on the growth of BDD films and have less effect on the grain size.

The decrease in grain size of BDD films leads to a significant increase in the number of grain boundaries and more precipitation of sp^2 phases at the grain boundaries[37]. More grain boundaries and more sp^2 phase will lead to more defects, thus a better activity of the BDD electrode[38], higher surface energy, and enhanced hydrophilicity and adsorption of the film[39]. It will also reduce the quality of BDD films, worsening the corrosion resistance and stability, and reducing their lifetime.

Figures 2a-6 show SEM images of ultra-heavy doped BDD film. Part of the BDD film loses the grain morphology of diamond and turns into a rod-like amorphous structure [40, 41]. This is due to the formation of a large number of borohydride compounds when the concentration of B_2H_6 is high, which hinders the further growth of diamond. Meanwhile, B_2H_6 reduces the etching of the graphite phase by atomic H, resulting in the growth of a large amount of amorphous and sp^2 phase carbon, which greatly reduces the quality of BDD films[41].

The standard B-doping characteristic peaks[42], diamond phase and graphite phase characteristic peaks[43] are at 400 - 600 cm^{-1}, 1332 cm^{-1} and 1580 cm^{-1}, respectively. The Raman spectrum is shown in Fig. 2b. Among them, the ultra-light doped BDD film prepared with B_2H_6 gas flow rate of 0 sccm also has characteristic peaks associated with B doping, this adventitious B is likely due to a small amount of B residue in the reactor chamber and gas pipeline during the long-term use of the HFCVD equipment. With the increase of B doping concentration, the diamond characteristic peaks of BDD films shifted to the left. This is due to the substitution of B atoms with an atomic radius larger than C atoms into the diamond crystal, which will cause the expansion of the diamond lattice and greatly increase the tensile stress of the BDD film[44]. With the increase of B doping concentration, the widening of the diamond peak shape was observed, changing from a sharp peak shape to a hump, which indicates the decrease in the crystal quality of the BDD film. This is because the increase in the doping

concentration of the B element will greatly increase the defects in the diamond lattice. The more crystal defects, the shorter the lifetime of the phonon and the wider the peak width[45]. The ultra-heavy doped diamond shows an obvious peak shift indicating large internal stress of diamond, deterioration of crystal lattice, increase of defects, and decrease of the quality of diamond film.

When the doping concentration is from ultra-light to heavy, there is no obvious peak at the characteristic peak location of the graphite phase in the Raman spectrum, while there is an obvious peak of graphite for ultra-heavy B-doped BDD film, which is consistent with the SEM image results. With the increase of B content, the B doping correlation peak gradually shifted to the left, and the Lorentzian-Gaussian fitting method was used to calculate the wavenumber W corresponding to the B doping correlation peak of the Lorentzian component in the Raman spectrum. According to formula (6), the actual concentration of B atoms incorporated in a unit cubic centimetre [B] in the BDD film can be calculated[46].

$$[B] = 8.44 \times 10^{30} \times \exp(-0.048W) \quad (6)$$

Figure 2d shows that with the increase of the B_2H_6 gas ratio, the B doping level in the BDD film increases significantly, and the B doping concentration of the ultralight, light, medium, heavy and ultra-heavy doped BDD films is 1.1×10^{19}, 12.3×10^{19}, 159.1×10^{19}, 258.3×10^{19} and751.6×10^{19} cm^{-3}. From ultra-light doping to medium doping, the B doping concentration of BDD films increases significantly (more than 10 times). From medium doping to ultra-heavy doping, the rate of increase of B doping concentration in BDD films slows down due to a critical doping concentration of B atoms in diamond as diamond film is limited by the crystal lattice[44].

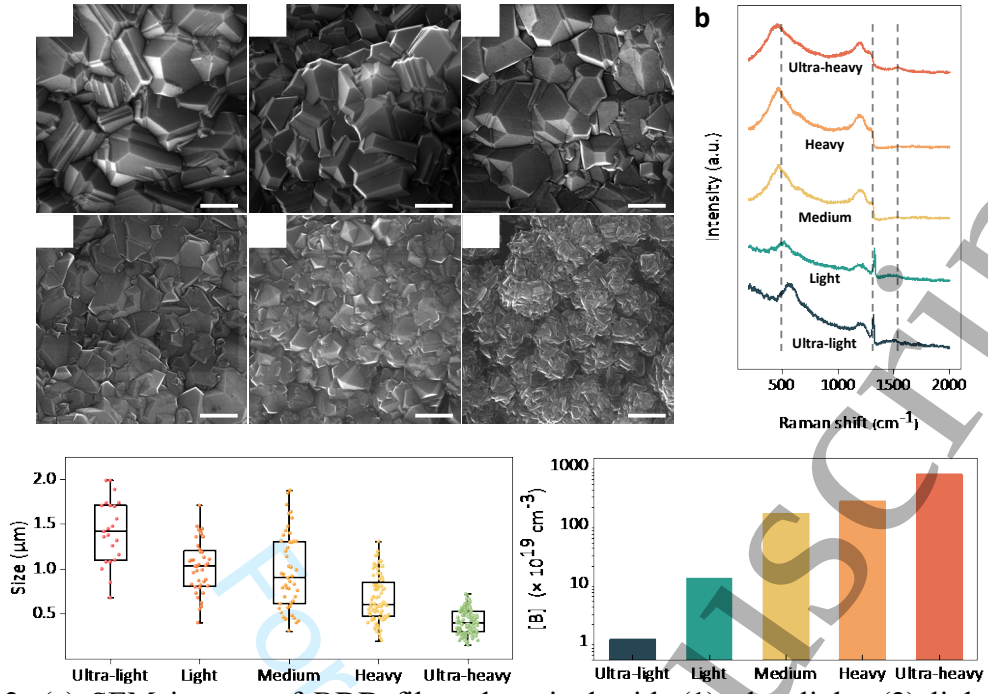

Fig. 2. (a) SEM images of BDD films deposited with (1) ultra-light, (2) light, (3) medium, (4) heavy, and (5)-(6) ultra-heavy B doping, respectively. (b) The Raman spectra, (c) grain size results and (d) the boron doping concentration of BDD films deposited with different boron concentrations, respectively.

3.2 Electrochemical properties of BDD Electrodes

The electrochemical properties such as oxygen evolution potential, charge transfer resistance, and EASA can explain how the physical and chemical properties of the BDD film affect the final electrochemical oxidation performance of the electrode[45].

The oxygen evolution potential (OEP) can directly reflect the difficulty of the oxygen evolution side reaction of the electrode, and it is an important indicator of the electrochemical oxidation capacity of electrode materials. The higher the oxygen evolution potential of the electrode, the less the side reaction of oxygen evolution occurs, which is more favourable to the electrochemical oxidation of other substances[47]. The CV curves of BDD electrodes were tested as shown in Figure 3-a. The oxygen evolution potential of the electrode is determined by making a tangent to the oxygen evolution reaction peak. The potential corresponding to the intersection of the tangent and the charging current is the oxygen evolution potential of the electrodes as shown in Figure 3a. The oxygen evolution potentials of the ultra-light, light, medium, heavy and ultra-heavy doped BDD films were 2.41, 2.38, 2.36, 2.35, 2.22 V (vs. Ag/AgCl), respectively (Table 1). With the increase of B doping level, from ultra-light to heavy,

the oxygen evolution potential of the electrode decreased, which is due to the decrease of diamond grain size, the increase of grain boundaries, and the increase of sp^2 impurities which promote the electrode activity[39]. The increased surface energy enhanced the adsorption of ·OH, and hindered the free ·OH, promoting the reaction to generate O_2 by combining two ·OH. At the same time, with the increase of B doping concentration, there were more boron-rich sites on the surface of the BDD film, and the adsorption of water molecules became stronger, which is also conducive to the oxygen evolution reaction. For ultra-heavy doped BDD, the oxygen evolution potential of the electrode was greatly reduced, which is likely due to the poor quality of the BDD film, the loss of diamond morphology, and the significant increase of the sp^2 impurity phase[48].

The EIS of the BDD electrode was measured in 1 mM $K_4[Fe(CN)_6]/K_3[Fe(CN)_6]$ + 1 M KCl solution as shown in Fig. 3b. The equivalent circuit for fitting the EIS data (Figure 3b inset) consists of system internal resistance (R_s), electric double-layer capacitance, charge transfer resistance (R_{ct}) and mass transfer impedance (Z_w)[48]. R_s mainly refers to the contact resistance between the electroactive material and the current collector and the ionic resistance of the electrolyte solution. Constant phase element (CPE) was used to represent double layer capacitance due to the rough surface of BDD electrodes or inhomogeneous distribution of active sites[48].With the increase of B doping, the inhomogeneity of the atomic scale of the film surface intensifies, the diamond grain size decreases, and the surface microroughness of the BDD film increases, which makes the value of CPE gradually increase[48]. The value of R_{ct} represents the ease of charge transfer from the electrode material to the electrolyte solution, and the values are shown in Fig. 3c. The R_{ct} gradually decreases with increasing B doping concentration, which indicates that the charge transfer from the BDD surface to the electrolyte became easier. Among them, Z_w is mainly related to the diffusion rate of redox pairs in electrochemical tests[49].

The concept of EASA characterises the actual surface area of the electrode that participates in the electrochemical catalytic reaction, thereby evaluating the real catalytic activity of the electrode material. As shown in Fig. 3d and S1, with the increase of the scan rate, the peak current of the BDD electrode increased and the potential of the oxidation peak shifts to the right, and the separation of the potentials between the oxidation and reduction peaks became larger. This is because, at a high scan rate, the current flow increased and the ohmic drop in the solution increased, requiring a higher

overpotential to reach the peak current. The peak current increased from ultra-light to heavy B doped BDD, which is associated with the increase of B doping content of BDD films[50] and the increase of the sp^2 phase, promoting the activity of the electrode and the conductivity of the film[49]. This finding is consistent with the results of the charge transfer resistance analysis. When the B doping concentration changes from heavy to ultra-heavy, the peak current decreased instead. This is due to the poor quality of the BDD film caused by ultra-heavy doping[35], the appearance of rod-shaped amorphous structure, a large amount of boron dimers and sp^2 impurity phase (due to grain size reduction), improving the sheet resistance.

To detect the EASA of the electrodes, a linear fit was performed using the peak currents (including the anodic peak current and the cathodic peak current) against the root mean square of the scan rate (Figures 3e and S2). The coefficients of determination R^2 of the linear fitting are all above 0.99, which indicates that in the $[Fe(CN)]^{3-/4-}$ system, a quasi-reversible electrochemical reaction occurred on the surface of the BDD thin film electrode, and the whole reaction is a diffusion-controlled mass transfer process. The slope (k) of the fitted line of the BDD electrode can semi-quantitatively contrast the EASA of the electrodes with different B doping concentrations.

The results show that with the increase of the B doping concentration, the fitting slope gradually increased, which represents the increase of the EASA of the electrodes. This could be attributed to the higher the B doping concentration, the lower the diamond grain size, the more sp^2 phase and surface defects, increasing the electrochemical activity of the electrode. At ultra-heavy doped BDD, the slope *k* is greatly increased, which is attributed to the poor quality of BDD films with more impurities and defects[35]. Compared with the inert sp^3 structure of diamond, the bonding energy of the impurity phase is lower and the energy is higher, which greatly improves the activity of the BDD electrodes.

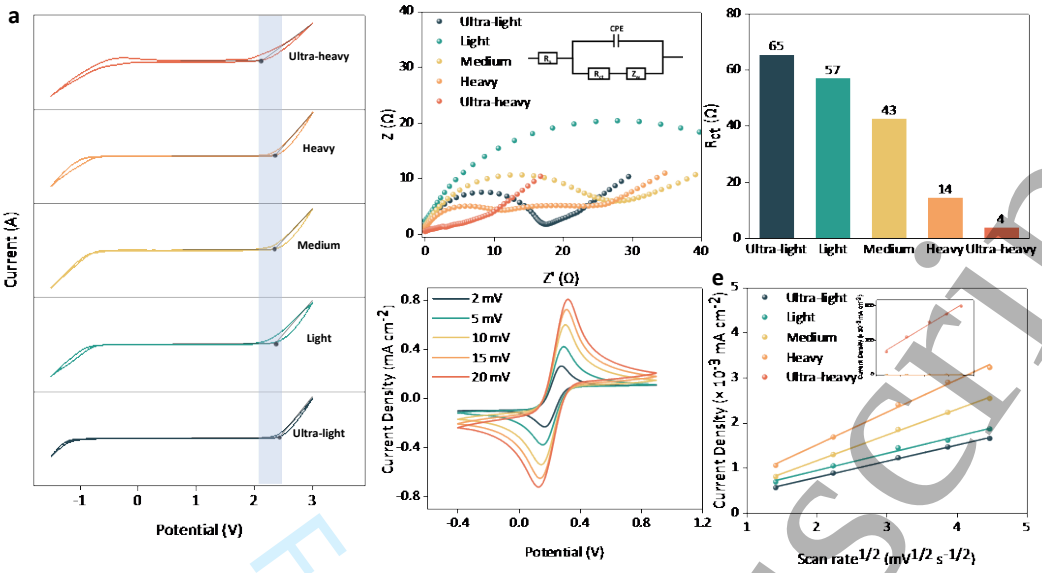

Fig. 3 (a) The CV curves, (b) EIS and (c) R_{ct} of BDD films with ultra-light, light, medium, heavy, and ultra-heavy B doping concentration, respectively. (d) CV curves of 2, 5, 10, 15, and 20 mV s^{-1} scan rates were measured at boron-doped BDD electrodes with heavy boron doping concentrations in the 1 mM $K_4[Fe(CN)_6]/K_3[Fe(CN)_6]$ + 1 M KCl redox system. (e) The linear fits of peak anode currents and the root mean square of the scan rate for ultra-light, light, medium, heavy, and ultra-heavy B doping concentration BDD electrodes, respectively.

Table 1 The Electrochemical properties of BDD electrodes with different boron doping Concentrations

	Ultra-light	light	medium	heavy	Ultra-heavy
OEP (V)	2.41	2.38	2.36	2.35	2.22
Slope k (× 10^{-3})	3.59	3.79	5.72	7.23	1280
CPE (μF)	4.23	17.52	23.12	234.11	418.91
R_{ct} (Ω)	65.34	56.99	42.61	3.83	3.93
Z_W (× 10^{-2} Ω)	1.76	2.53	2.22	7.94	7.65

3.3 The variation of electrochemical oxidation products of BDD electrodes over time

To explore the effect of B doping concentration on the electrochemical oxidation performance, the yields of ClO_3^- and ClO_4^- on BDD electrodes in water containing Cl^-, electrochemical oxidation experiments were conducted in 0.1 M NaCl solution. The experiments were carried out at a current density of 50 mA cm^{-2}. The AC produced in the reaction can be widely used in wastewater degradation, and electro-oxidative disinfection and its yield can reflect the electrochemical oxidative degradation ability of the BDD electrode in chlorine-containing water.

We first analysed the lightly doped BDD electrode with the highest AC yield. Figure 4a shows the reaction product concentrations at different times for lightly doped BDD electrodes. The concentration of AC increased first and then decreased with time, reaching a maximum of 681.73 mg L^{-1}, while the concentrations of ClO_3^- and ClO_4^- increased gradually with time, and finally reached 180.73 mg L^{-1} and 40.27 mg L^{-1}, respectively. In the initial stage of the experiment, the anions in the solution were mainly Cl^-, and Cl^- was adsorbed on the surface of the BDD electrode and then largely desorbed after oxidized to AC by ·OH. Only a small amount of AC was still adsorbed on the surface of BDD and further oxidized to ClO_3^- and even ClO_4^-. In the middle and late stages of the experiment, the concentration of Cl^- in the solution was greatly reduced, which slowed down the generation of AC, while the higher concentration of AC increased the generation rate of ClO_3^-. In addition, when the concentration of AC is high, some AC will escape from the solution in the form of Cl_2, ClO_2, etc., resulting in a decrease in its concentration.

From the perspective of efficiency and energy consumption, the current efficiency of the BDD electrodes to generate AC, total chlorine, and the unit energy consumption of AC were calculated and the results are shown in Figure 4b and c. The current efficiencies of AC and total chlorine increased first and then decreased with time, and the highest was 54.54% and 85.02%, respectively. This could be ascribed to the fact that at the early stage of the experiment, the types and concentrations of chlorine-containing species in the solution increased with time, which would compete with side reactions such as oxygen evolution, thereby improving the current efficiency. Meanwhile, ≡C-O· and =C·OH sites were generated during electrochemical oxidation of BDD films, which will facilitate the adsorption of chlorine and further oxidation

reactions[22]. In the later stage of the reaction, the types and concentration of chlorine-containing species gradually decreased, and part of the AC escaped from the solution, resulting in a decrease in the current efficiency. Figure 4c shows the unit energy consumption for producing AC which first decreased and then increased with time, reaching a minimum of 10.38 kWh kg^{-1}, which is consistent with the current efficiency results.

Figure 4d shows the time-dependent current efficiency curves for the generation of ClO_3^- and ClO_4^-. The current efficiencies of generating ClO_3^- and ClO_4^- both increased with time, reaching a maximum of 29.02% and 7.24%, respectively. This is because, there were more high-valent AC in the solution and less low-valent chlorine with the progress of electrochemical oxidation experiments, which resulted in a continuous increase of the generation rate of ClO_3^- and ClO_4^-.

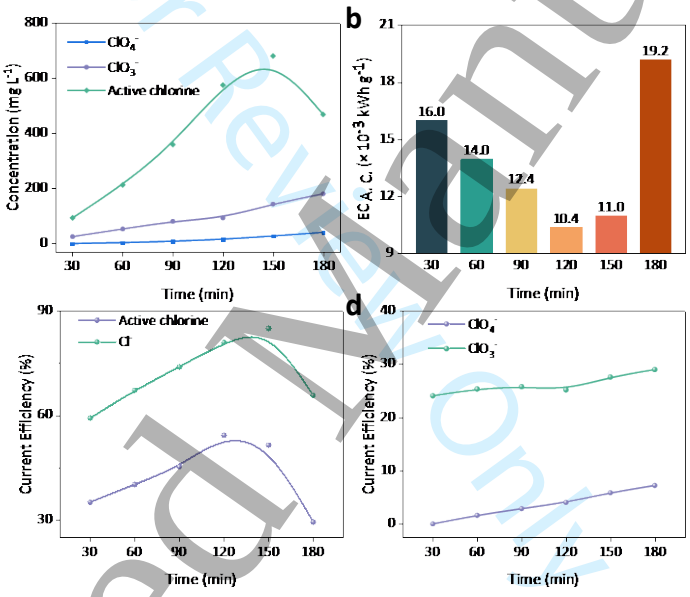

Fig. 4 (a) The concentration of reaction products at different times for BDD electrodes with low doping concentration. (b) The variation of energy consumption per unit gram of AC with time. (c) The current efficiency of AC and total chlorine. (d) The current efficiency of ClO_3^- and ClO_4^-.

3.4 Effect of B Doping Concentration on Electrochemical Oxidation of Cl^-

Figure S3 shows the concentration of AC, ClO_3^- and ClO_4^- produced by electrochemical oxidation at BDD electrodes with different B doping concentrations, where the concentrations of ClO_3^- and ClO_4^- both increased with time. It is also observed that low B doping BDD facilitated the production of AC while high B doping eased the formation of ClO_3^- and ClO_4^-, and lightly doped BDD yielded the highest AC

concentration (over 600 ppm at 150 min). During the electrochemical oxidation process, the cell voltages of BDD electrodes with different B doping concentrations are shown in Fig. 5a, in which the inset is a comparison of images of electrodes with different B doping concentrations. With the increase of B doping concentration, the cell voltage first decreases and then increases. This could be attributed to the fact that with the increase in B doping amount, the charge transfer resistance of the electrode gradually decreased, the EASA gradually increased, and the cell voltage gradually decreased. For ultra-heavy doped BDD, the SEM image and Raman spectrum show that there are a large amount of defects and impurities (non-sp^3 phases), which undermines the electrical conductivity of the BDD film and leads to the increase of the cell voltage in the constant current mode.

The current efficiency is an important index to evaluate the proportion of electrode reaction. Figure 5c shows the current efficiency to generate AC and total chlorine (Cl) during the electrochemical oxidation using BDD electrodes with different B doping concentrations. Current efficiencies for generating AC and total chlorine with BDD electrolysis first decreased and then increased, and current efficiency was the lowest with the heavily doped BDD electrode. This is owing to the gradual decrease of the oxygen evolution potential and the gradual increase of the current efficiency of the side reaction of oxygen evolution from ultra-light doping to heavy doping, resulting in a continuous decrease in the current efficiency of AC and total chlorine generation. For ultra-heavy doped BDD, the high concentration of B_2H_6 during the deposition process resulted in a large number of impurity phases such as boron dimer on the surface of the film[51], which significantly changes the electrochemical oxidation performance of the BDD film[52], enhances the adsorption of Cl^- on BDD and promotes the reactivity of BDD towards Cl^- thus increasing the current efficiency for generating AC and total chlorine.

To further compare the ability to produce AC using BDD electrodes with different B doping levels, the minimum energy consumption required for each BDD electrode to generate a unit mass of AC was compared as shown in Figure 5b. The minimum energy consumption required to generate a unit gram of AC first decreased and then increased with the increase of the B doping level. This is because, with the increase of B doping concentration, the overall energy consumption of the electrochemical oxidation system first decreased and then increased in constant current mode. Therefore, the lowest

energy consumption was obtained with the medium doped BDD electrode instead of the heavily doped BDD electrode with the lowest cell voltage.

The relationship between the final concentration of ClO_3^- and corresponding current efficiency and B doping level was explored (Fig. 5d). ClO_3^- is an intermediate valence species, which can be generated in various ways during the electrochemical oxidation of BDD electrodes. For example, the adsorbed AC reacts with hydroxyl radicals to generate $ClO_2\cdot$, and then $ClO_2\cdot$ reacts with ·OH to generate ClO_3^-[22]. At the same time, some high-valence AC can also generate ClO_3^- via disproportionation reactions. Generally, the ClO_3^- yield is mainly affected by the concentration of AC and the generation rate of ClO_4^-. With the increase of B doping concentration, the generation rates of AC and ClO_4^- both decreased at first and then increased. The combined effect of these two led to the production of ClO_3^- decrease first and then increase with the increase of B doping concentration. Among them, the concentration of highly doped BDD electrodes is the lowest, and the yields of lightly doped and medium doped BDD electrodes are close.

Compared with other electrodes when used in electrochemical oxidation, the BDD electrode will generate a large amount of ClO_4^-, which has attracted the attention of researchers. It is believed that the ClO_4^- is generated by a two-step reaction as shown in formulas (1) and (2)[22].

Firstly, ClO_3^- adsorbed on the BDD electrode and oxidized to ClO3·, which is mainly controlled by the adsorption of ClO_3^- on the surface of the BDD film, that is, controlled by the production of ClO_3^-, its adsorption capacity of the BDD surface and the EASA. The second step is that $ClO_3\cdot$ reacts with ·OH to generate ClO_4^-, which is controlled by the yield of free ·OH, so it is mainly controlled by electrode mass transfer and the space-time yield of ·OH. The first reaction is difficult to occur on the BDD electrode and the reaction rate is slow, so the ClO_3^- reaction to generate ClO_4^- is mainly limited by the yield of ClO_3^-, its adsorption of BDD film and the electrode EASA. Factors such as mass transfer, surface terminal groups and Cl^- concentration will also have a greater impact on the yield of ClO_4^- and their effects were eliminated as much as possible through electrode structure control and anodic polarization. Herein, the effect of the doping concentration of B on BDD film and the yield of ClO_4^- were explored.

Figures 5e and f show the concentration and current efficiency of ClO_4^- produced

by BDD electrodes with different B doping concentrations. The ClO_4^- production of all BDD electrodes increased with time, which is consistent with the previous results. The relationship between boron doping level and the ClO_4^- concentration is that the ClO_4^- concentration increases with boron doping level from the light doped to ultraheavy doped electrodes, while the ClO_4^- concentration of the ultralight doped electrode is in the middle of the medium and heavy doped. This trend also applies to the relationship between the boron doping level and current efficiencies (Fig. 5f).

Among them, the concentration and current efficiency of ClO_4^- generated from ultra-light doped BDD electrodes are higher, which can be ascribed to the higher ClO_3^- yield enhanced the yield of ClO_4^-. From lightly doped to heavily doped BDD electrodes, the concentration of ClO_4^- and current efficiency of BDD electrodes gradually increased. This trend can be attributed to the continuous increase of EASA and surface energy of BDD electrodes with the increase of B doping concentration, which is beneficial to the adsorption of ClO_3^- on the electrode surface to generate $ClO_3^{\cdot}$, thereby increasing the yield of ClO_4^-. The ultra-heavy doped BDD electrode also showed a significant increase in ClO_4^- yield to the highest value due to its surface energy, EASA and ClO_3^- yield. Overall, the concentration and current efficiency of ClO_4^- generated from light-doped BDD electrodes are relatively low which is highly safe.

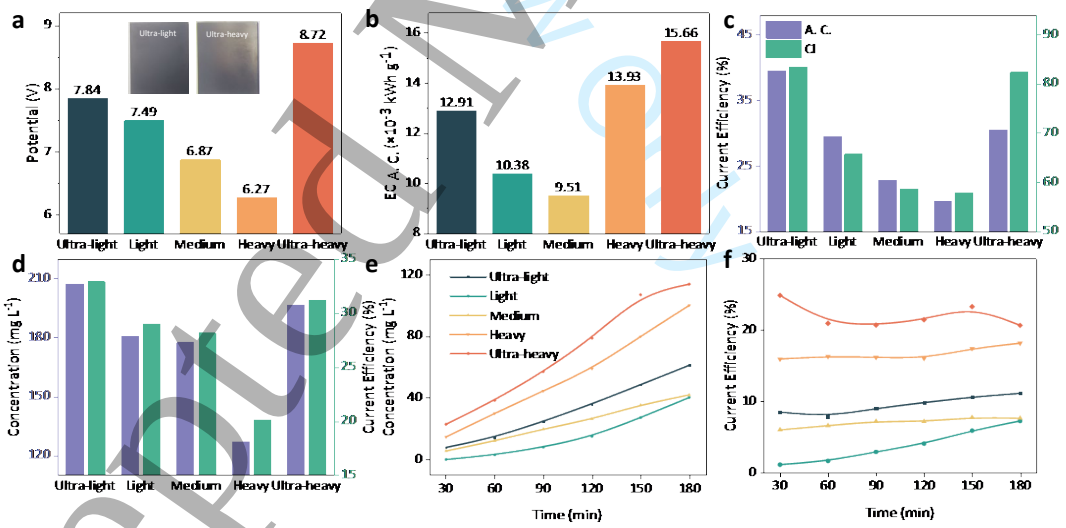

Fig. 5 (a) The average tank voltage of BDD electrodes with ultra-light, light, medium, heavy, and ultra-heavy B doping concentration, respectively. (b) The minimum energy consumption required per unit of AC of BDD electrodes; (c) The current efficiency of active and total chlorine of BDD electrodes. (d) The final yield and current efficiency of ClO_3^- of BDD electrodes. (e) The ClO_4^- yield and (f) current efficiency of BDD electrodes with ultra-light, light, medium, heavy, and ultra-heavy B doping

concentration, respectively.

3.5 Effect of B doping concentration on electrochemical oxidation and degradation of organic matter

In this work, TC and GLu were used as simulated organic pollutants for electrochemical oxidative degradation using lightly doped and ultra-heavy doped BDD electrodes. Figure 6a and b show the final concentrations of ClO_3^- and ClO_4^- during the degradation using these two BDD electrodes in Cl^- containing solutions. For TC and GLu solutions, the final concentrations of ClO_3^- were 109.92 and 123.01 mg L^{-1}; and final concentrations of ClO_4^- were 28.58 and 11.29 mg L^{-1} for lightly doped BDD electrodes. The final concentrations of ClO_3^- in the ultra-heavy doped BDD electrode were 183.35 and 219.84 mg L^{-1}, respectively, which are 1.67 and 1.79 times that of the lightly doped electrode. The final ClO_4^- concentrations were 73.16 and 44.24 mg L^{-1}, respectively, which are 2.56 and 3.92 times that of the lightly doped electrodes. This shows that the B doping concentration has a great influence on the ClO_3^- and ClO_4^- concentrations generated by the BDD electrode when degrading organic substances. Ultra-heavy doped BDD generated much more ClO_3^- and ClO_4^- compared to lightly doped BDD during the electrolysis which is in accordance with a previous finding that BDD electrode with lower sp3/sp2 ratio facilitates the production of ClO_4^-[30].

Compared with the NaCl solution without organic substances, the concentration of ClO_3^- and ClO_4^- produced were lower. This is because the degradation reactions of TC and Glu are competing with the oxidation reactions of AC to produce ClO_3^- and ClO_4^-. On one hand, the indirect oxidation of organic substances will consume AC and hydroxyl radicals, reducing the rate of further oxidation of AC. On the other hand, direct oxidation of the organic substances would occupy the active sites on the electrode surface, limiting the active sites for direct oxidation of AC. . Compared with the easily oxidized GLu with a simple structure, the concentrations of ClO_3^- and ClO_4^- produced in TC solution were higher, and the concentration of ClO_4^- was about 2 times higher. This is due to the higher oxidation potential of TC, which has a complex and stable structure. TC and its intermediates are difficult to be directly oxidized by the BDD electrode and oxidized by AC, which leads to the increase of ClO_3^- and ClO_4^- concentrations.

The UV spectra of TC and GLu degradation by using the BDD electrode are shown in Figure 6c, d and S4, in which TC has an obvious UV absorption peak at 275 and 357

nm[48], while GLu has no UV absorption peak. During electrochemical degradation, TC was rapidly oxidized first and completely degraded within 90 min. After that, new UV absorption peaks appeared and the intensities increased with the degradation time, which is associated with some intermediate products containing toxic chlorinated products. The UV spectrum in GLu solution also showed a new UV absorption peak during the degradation process, which was consistent with TC.

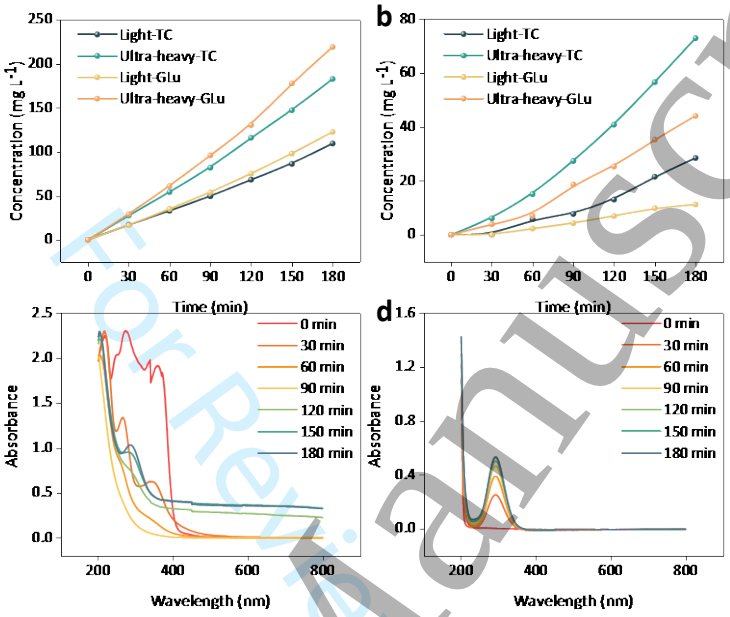

Fig. 6 (a) ClO_3^- and (b) ClO_4^- concentrations produced by light and ultra-heavy doped BDD electrodes during electrochemical oxidative degradation of TC and GLu in Cl^- containing solutions. UV-vis spectra of electrochemical oxidative degradation of (c) TC and (d) GLu at lightly doped BDD electrodes in Cl^- containing solutions.

4. Conclusion

In this work, the effects of B doping concentration on the macro-microstructure and electrochemical performance of BDD electrodes were studied, and the mechanism of B doping concentration on the types and concentrations of electrochemically oxidized Cl^- products were explored. With the increase of B doping concentration, the grain size of the diamond decreased from 1.42 μm to 0.4 μm with rougher surface and more defects,. the OEP decreases from 2.41 V to 2.22 V (vs. Ag/AgCl), the charge transfer resistance of the electrode gradually decreases, and the EASA gradually increases.

In NaCl solution electrolysis experiments, with the increase of B doping concentration, the current efficiency of generating AC first increased and then

decreased, the minimum energy consumption required to generate unit AC decreased first and then increased, and the energy consumption of lightly doped BDD electrode was the lowest. The yield and current efficiency of producing ClO_4^- decreased first and then increased, and the lightly doped BDD (B doping concentration 1.23×10^{20} cm^{-3}) reached the lowest. In the simulated wastewater degradation experiments, the lightly doped BDD electrodes showed less production of ClO_3^- and ClO_4^-. In general, lightly doped BDD shows the best overall electrochemical oxidation performance with high yield of AC, low energy consumption to produce AC and low yield of ClO_3^- and ClO_4^-. This work offers an easy way to control the production of chlorine electrolysis on BDD electrodes, promoting the safe and efficient use of BDD electrode for chlorinated wastewater treatment.

Acknowledgments

We gratefully acknowledge the National Key Research and Development Program of China (No.2021YFB3701800, No. 2016YFB0301400), the National Natural Science Foundation of China (No. 52071345, No. 51874370), the Province Key Research and Development Program of Guangdong (No. 2020B010185001), the Province High-tech Industry Science and Technology Innovation Leading Plan of Hunan (No. 2022GK4037, No. 2022GK4047) and the State Key Laboratory of Powder Metallurgy for financial support.

References

1. M. Rajab, C. Heim, T. Letzel, J. E. Drewes, and B. Helmreich, *Chemosphere,* **121** 47-53 (2015).
2. R. E. Palma-Goyes, J. Silva-Agredo, J. Vazquez-Arenas, I. Romero-Ibarra, and R. A. Torres-Palma, *J. Environ. Chem. Eng.,* **6** (2), 3010-3017 (2018).
3. D. Ghime and P. Ghosh, *Russ. J. Electrochem.,* **55** (7), 591-620 (2019).
4. C. A. Martínez-Huitle and M. Panizza, *Current Opinion in Electrochemistry,* **11** (2018).
5. K. C. D. Araujo, D. R. da Silva, E. V. dos Santos, H. Varela, and C. A. Martinez-Huitle, *J. Electroanal. Chem.,* **860** 7 (2020).
6. X. L. Li, D. Shao, H. Xu, W. Lv, and W. Yan, *Chem. Eng. J.,* **285** 1-10 (2016).
7. Y. P. He, H. B. Lin, Z. C. Guo, W. L. Zhang, H. D. Li, and W. M. Huang, *Sep. Purif. Technol.,* **212** 802-821 (2019).
8. Y. He, X. Wang, W. Huang, R. Chen, W. Zhang, H. Li, and H. Lin, *Chemosphere,* **193** 89-99 (2018).
9. D. Deng, X. Wu, M. Li, S. Qian, B. Tang, S. Wei, and J. Zhang, *Chemosphere,* **259** 127488 (2020).
10. P. Kariyajjanavar, J. Narayana, and Y. A. J. J. o. E. C. E. Nayaka, **1** (4), 975-980 (2013).
11. E. Pajootan and M. J. E. A. Arami, **112** 505-514 (2013).
12. F. L. Souza, C. Saez, M. R. V. Lanza, P. Canizares, and M. A. Rodrigo, *Appl. Catal. B-Environ.,* **180** 733-739 (2016).
13. B. P. Chaplin, I. Wyle, H. J. Zeng, J. A. Carlisle, and J. Farrell, *J. Appl. Electrochem.,* **41** (11), 1329-1340 (2011).
14. D. T. Miao, T. Liu, Y. L. Yu, S. B. Li, G. S. Liu, Y. H. Chen, Q. P. Wei, K. C. Zhou, Z. M. Yu, and L. Ma, *Appl. Surf. Sci.,* **514** 10 (2020).
15. M. Panizza and G. Cerisola, *Chem. Rev.,* **109** (12), 6541-6569 (2009).
16. M. A. Ajeel, T. A. A. Hassan, A. S. Naje, and M. K. T. Aroua, *J. Environ. Chem. Eng.,* **6** (4), 3884-3888 (2018).
17. N. Bensalah, M. F. Ahmadi, and C. A. Martinez-Huitle, *Sep. Purif. Technol.,* **263** 9 (2021).
18. C. A. Martinez-Huitle, M. A. Rodrigo, I. Sires, and O. Scialdone, *Chem. Rev.,* **115** (24), 13362-13407 (2015).
19. R. C. Jackson, W. J. Elder, and H. McDonnell, *Lancet (London, England),* **2** (7217), 1381-1383 (1961).
20. W. J. Feng, A. Deletic, Z. Y. Wang, X. W. Zhang, T. Gengenbach, and D. T. McCarthy, *Sci. Total Environ.,* **646** 1440-1447 (2019).
21. H. Zollig, A. Remmele, C. Fritzsche, E. Morgenroth, and K. M. Udert, *Environ. Sci. Technol.,* **49** (18), 11062-11069 (2015).
22. D. K. Hubler, J. C. Baygents, B. P. Chaplin, and J. Farrell, *J. Electrochem. Soc.,* **161** (12), E182-E189 (2014).
23. O. Azizi, D. Hubler, G. Schrader, J. Farrell, and B. P. Chaplin, *Environ. Sci. Technol.,* **45** (24), 10582-10590 (2011).
24. Y. J. Jung, K. W. Baek, B. S. Oh, and J. W. Kang, *Water Res.,* **44** (18), 5345-5355 (2010).
25. M. E. H. Bergmann, J. Rollin, and T. Iourtchouk, *Electrochimica Acta,* **54** (7), 2102-2107 (2009).
26. I. Moraleda, S. Cotillas, J. Llanos, C. Saez, P. Canizares, L. Pupunat, and M. A.

Rodrigo, *J. Electroanal. Chem.,* **850** 7 (2019).
27. P. Gayen and B. P. Chaplin, *ACS Appl. Mater. Interfaces,* **9** (33), 27638-27648 (2017).
28. W. Jawando, P. Gayen, and B. P. Chaplin, *Electrochim. Acta,* **174** 1067-1078 (2015).
29. F. L. Souz, C. Saez, M. R. V. Lanza, P. Canizares, and M. A. Rodrigo, *Electrochim. Acta,* **187** 119-124 (2016).
30. C. D. Brito, D. M. de Araujo, C. A. Martinez-Huitle, and M. A. Rodrigo, *Electrochem. Commun.,* **55** 34-38 (2015).
31. G. O. S. Santos, K. I. B. Eguiluz, G. R. Salazar-Banda, C. Saez, and M. A. Rodrigo, *J. Electroanal. Chem.,* **857** 8 (2020).
32. I. Duo, C. Levy-Clement, A. Fujishima, and C. Comninellis, *J. Appl. Electrochem.,* **34** (9), 935-943 (2004).
33. D. T. Miao, Z. S. Li, Y. H. Chen, G. S. Liu, Z. J. Deng, Y. L. Yu, S. B. Li, K. C. Zhou, L. Ma, and Q. P. Wei, *Chem. Eng. J.,* **429** 9 (2022).
34. R. Q. Mei, Q. P. Wei, C. W. Zhu, W. T. Ye, B. Zhou, L. Ma, Z. M. Yu, and K. C. Zhou, *Appl. Catal. B-Environ.,* **245** 420-427 (2019).
35. N. G. Ferreira, E. Abramof, E. J. Corat, and V. J. Trava-Airoldi, *Carbon,* **41** (6), 1301-1308 (2003).
36. R. Bogdanowicz, A. Fabianska, L. Golunski, M. Sobaszek, M. Gnyba, J. Ryl, K. Darowicki, T. Ossowski, S. D. Janssens, K. Haenen, and E. M. Siedlecka, *Diam. Relat. Mat.,* **39** 82-88 (2013).
37. S. Wang, V. M. Swope, J. E. Butler, T. Feygelson, and G. M. Swain, *Diamond & Related Materials,* **18** (4), 669-677 (2009).
38. A. E. Fischer, Y. Show, and G. M. Swain, *Analytical Chemistry,* **76** (9), 2553 (2004).
39. X. L. Gao, W. Li, R. Q. Mei, C. W. Zhu, B. Zhou, L. Ma, Q. P. Wei, and T. Liu, *J. Electroanal. Chem.,* **832** 247-253 (2019).
40. A. F. Azevedo, M. R. Baldan, and N. G. Ferreira, *J. Phys. Chem. Solids,* **74** (4), 599-604 (2013).
41. I. Gerger and R. Haubner, *Int. J. Refract. Met. Hard Mat.,* **26** (5), 438-443 (2008).
42. Q. Wei, G. Liu, C. Zhu, B. Zhou, R. Mei, L. Ma, L. Zhang, W. Yang, W. Ye, K. Zhou, and Z. Yu, *Chemical Engineering Journal,* **397** 125465 (2020).
43. A. C. Ferrari and J. Robertson, *Physical Review B,* **63** (12), 121405 (2001).
44. Y. J. Feng, J. W. Lv, J. F. Liu, N. Gao, H. Y. Peng, and Y. Q. Chen, *Appl. Surf. Sci.,* **257** (8), 3433-3439 (2011).
45. J. V. Macpherson, *Phys. Chem. Chem. Phys.,* **17** (5), 2935-2949 (2015).
46. R. Ramamurti, M. Becker, T. Schuelke, T. Grotjohn, D. Reinhard, G. Swain, and J. Asmussen, *Diam. Relat. Mat.,* **17** (4-5), 481-485 (2008).
47. C. Comninellis, A. Kapalka, S. Malato, S. A. Parsons, L. Poulios, and D. Mantzavinos, *J. Chem. Technol. Biotechnol.,* **83** (6), 769-776 (2008).
48. W. L. Yang, J. L. Tan, Y. H. Chen, Z. S. Li, F. M. Liu, H. Y. Long, Q. P. Wei, L. B. Liu, L. Ma, K. C. Zhou, and Z. M. Yu, *J. Alloy. Compd.,* **890** 10 (2022).
49. S. N. Chai, Y. J. Wang, Y. N. Zhang, H. Y. Zhao, M. C. Liu, and G. H. Zhao, *Appl. Catal. B-Environ.,* **237** 473-481 (2018).
50. L. Svorc, D. Jambrec, M. Vojs, S. Barwe, J. Clausmeyer, P. Michniak, M. Marton, and W. Schuhmann, *ACS Appl. Mater. Interfaces,* **7** (34), 18949-18956 (2015).
51. E. Bourgeois, E. Bustarret, P. Achatz, F. Omnes, and X. Blase, *Phys. Rev. B,* **74**

(9), 8 (2006).
52. R. Long, Y. Dai, M. Guo, L. Yu, B. B. Huang, R. Q. Zhang, and W. J. Zhang, *Diam. Relat. Mat.,* **17** (3), 234-239 (2008).